LBL-21212 c.2

Lawrence Berkeley Laboratory
UNIVERSITY OF CALIFORNIA

LAWRENCE BERKELEY LABORATORY
9 1986
LIBRARY AND

Presented at the Symposium on the Many Facets of Heavy Ion Fusion Reactions, Argonne, IL, March 23-26, 1986

COMPLEX FRAGMENT EMISSION FROM HOT COMPOUND NUCLEI

L.G. Moretto

March 1986

TWO-WEEK LOAN COPY
This is a Library Circulating Copy which may be borrowed for two weeks.

NUCLEAR SCIENCE DIVISION

LBL-21212 c.2

Prepared for the U.S. Department of Energy under Contract DE-AC03-76SF00098

DISCLAIMER

This document was prepared as an account of work sponsored by the United States Government. While this document is believed to contain correct information, neither the United States Government nor any agency thereof, nor the Regents of the University of California, nor any of their employees, makes any warranty, express or implied, or assumes any legal responsibility for the accuracy, completeness, or usefulness of any information, apparatus, product, or process disclosed, or represents that its use would not infringe privately owned rights. Reference herein to any specific commercial product, process, or service by its trade name, trademark, manufacturer, or otherwise, does not necessarily constitute or imply its endorsement, recommendation, or favoring by the United States Government or any agency thereof, or the Regents of the University of California. The views and opinions of authors expressed herein do not necessarily state or reflect those of the United States Government or any agency thereof or the Regents of the University of California.

LBL-21212

COMPLEX FRAGMENT EMISSION FROM HOT COMPOUND NUCLEI

L.G. Moretto

Nuclear Science Division
Lawrence Berkeley Laboratory
University of California
Berkeley, California 94720

This work was supported by the Director, Office of Energy Research, Division of Nuclear Physics of the Office of High Energy and Nuclear Physics of the U.S. Department of Energy under Contract DE-AC03-76SF00098.

COMPLEX FRAGMENT EMISSION FROM HOT COMPOUND NUCLEI

L.G. Moretto

Nuclear Science Division
Lawrence Berkeley Laboratory
University of California
Berkeley, California 94720

Abstract:

The experimental evidence for compound nucleus emission of complex fragments at low energies is used to interpret the emission of the same fragments at higher energies. The resulting experimental picture is that of highly excited compound nuclei formed in incomplete fusion processes which decay statistically. In particular complex fragments appear to be produced mostly through compound nucleus decay. In appendix a geometric-kinematic theory for incomplete fusion and the associated momentum transfer is outlined.

Introduction:

The idea that compound nuclei are entities relegated to the lower energy range of nuclear reactions is a myth and a legacy handed down to us by our nuclear forefathers. If indeed we were limited, as they were, to their sharp tools like protons or alpha particles, we would be well advised to stick to low energies in order to form compound nuclei. With our modern, blunter tools at our disposal like heavy ions, we have learned otherwise and now know better. As it turns out, the tendency of nuclear systems to undergo fusion seems to be all-pervasive, even in energy regions where one would not have expected it.

At least half of this conference is dedicated to subbarrier fusion and to its enhancement with respect to our past unimaginative predictions. In the remaining parts of this conference, the higher energy regime will be explored. It is my conviction, borne out of our own data and, I suspect, by plenty more, that the tendency of nuclear systems to undergo some sort of fusion is still quite strong in this region as well. It is certainly true enough that, on the basis of the abundant complex fragment production, theories have been aired which envisage

fancy non-fusion processes, like nuclear shattering[1] and liquid vapor equilibrium.[2] But, if I read the data correctly, Nature has already made mincemeat of those theories, having opted again in favor of compound nucleus formation and decay. I agree that this stubborn conservative attitude on Nature's part is lamentable. This may be attributable to the fact that Nature is not too well read. Had she but glanced at any of these fancy theories, I am sure She would not have hesitated to follow them.

All joking aside, the fact remains that most of the complex fragments, at least up to 50 MeV per nucleon bombarding energies, seem to arise from the statistical decay of a compound nucleus formed in an incomplete fusion process. This process of incomplete fusion, or massive transfer is not well understood nor well characterized as yet. It is interesting to study the predictions of a geometrical model regarding the kinematic thresholds and the mass and momentum transfers vs. impact parameters. The avid reader will find an outline of such a model in appendix.

Before diving head-first into the main subject of complex fragment formation at high energies, I will favor those of you who may still have a streak of incredulity by showing that very low energy compound nuclei can decay by emitting complex fragments. The comfort of this conviction will give us courage to enter the more modern energy range of 10–50 MeV per nucleon and will permit us to verify, if all goes well, that even at these higher energies, the compound nucleus mechanism for the production of complex fragments still reigns.

Complex fragments "de profundis" or near their compound emission threshold.

Why is it so hard to believe that complex fragments can be emitted by a compound nucleus? The reason lies, I think, in the fact that we have been taught two "distinct" ways of compound nucleus decay: evaporation of light particles like n, p, ^{4}He on one hand, and fission on the other. Yet it should not be too difficult to appreciate that the underlying connection between the two ways is the mass asymmetry

coordinate.[3] Consider, in the liquid drop picture, the saddle point configuration. One of its normal modes is the mass asymmetry mode. If we choose a given mass asymmetry, we can search for the saddle point with that constraint. The locus of all these conditional saddles I have called ridge line.[3] The potential energy surface looks schematically like it is shown in Fig. 1. A compound nucleus, confronted with this potential energy ridge, can choose any asymmetry it cares. Once the ridge is surmounted, the nucleus can descend towards the product region. In most cases, except near symmetry for heavy systems, the ridge configuration is so indented to be nearly degenerate with the scission configuration. In other words, once the ridge line is reached, the system is pretty much committed to the chosen mass asymmetry.

Why is it then, that complex fragments are not easily seen in low energy compound nucleus decay!? Since the rate of decay is approximately proportional to the level density at the ridge line $\rho(E - V(x)) \simeq \rho(E)\exp - \frac{V(x)}{T}$, fragments will appear most abundantly where V(x) is low. As shown in Fig. 2 in light systems this occurs at the extreme asymmetries (evaporation), while in heavier systems this can occur both at the extreme asymmetries (evaporation), and at symmetry (fission). In order to see the intermediate particles, one must look for them by beating the odds of their low cross sections.

We have studied the emission of complex fragments near threshold in the reaction ^{3}He + Ag.[4] The choice of ^{3}He speaks for the intense skepticism prevailing at the time of inception. We had to take precautions against the accusations of projectile fragmentation, deep inelastic processes and the like! To make a long story short let me show three figures. Figure 3 shows the invariant cross section for four different fragments. Notice the presence of a single source with compound nucleus velocity, and the Coulomb-like energies of the fragments. Figure 4 shows the excitation functions of a number of fragments. Any nuclear physicist worth his or her neutrons will see in their rapid rise with energy the unmistakable signature of compound nucleus mechanism. The lines through the points are fits from which one can obtain the conditional barriers as well as the a_z/a_n ratios. The latter ratio being one to within a couple of percent, let us look at the extracted barriers in

Fig. 5. The points are the experimental values, while the two lines, calculated by Sierk,[5] represent the liquid drop predictions and the prediction of a fancier model that includes finite range effects. For the non expert, these are due to the surface-surface interaction which becomes important for strongly indented shapes. The impressive agreement between the finite range calculation and the data speaks clearly to those who remember the role of fission barriers in establishing the liquid drop parameters. But this would tempt us to stray too far. So let us return to the main theme which is the appreciation of the compound nucleus mechanism as the source of complex particles. In order to satisfy ourselves that the yields do indeed reflect the topology of the ridge line, we have studied the reactions Be, C + Ge, Nb, La at 8.5 MeV per nucleon in reverse kinematics.[6]

Reverse kinematics helps a great deal in many ways. One of them is to lift the fragment kinetic energy so that, even if their rate is low, the products can be easily identified in a low background environment. Figure 6 shows an example of the center of mass kinetic energies which are Coulomb like and of the source velocities which do correspond to complete fusion. Figure 7 shows the cross sections vs. Z. For the first time we see the complete Z distributions and their agreement with the compound nucleus calculations based upon the liquid drop model. Notice the sudden appearance of a maximum at symmetry for the Be + La system indicating that we are now above the Businaro-Gallone point.

Plus, ça change, plus c'est la même chose, or: Compound nuclei forever?

Having established that complex fragments can be emitted by compound nuclei, and that at low energies they are only emitted by compound nuclei, the decision naturally came to see what is in fact going on at higher energies. Should any kind of compound nucleus be formed, it would decay abundantly by complex fragment emission due to its high excitation energy. This is the inescapable conclusion provided by statistical mechanics: if B_n and B_z are the neutron binding energy and the barrier for the fragment of charge Z respectively, and T the temperature, the ratio for the two decay rates is

$$\frac{\Gamma_z}{\Gamma_n} \simeq \exp - (B_z - B_n)/T$$

Taking $B_n \simeq 7$ MeV, $B_z \simeq 35$ MeV and $T = 5\text{–}6$ MeV one gets

$$\frac{\Gamma_z}{\Gamma_n} = \exp - \frac{28}{5\text{–}6} \simeq 10^{-2} \quad .$$

In other words, allowing for the contribution of the various isotopes and multiple chance emission, one could expect cross sections as large as several tens of millibarns per Z, or more if we allow for angular momentum effects. The corollary of this is that any additional "fancy" mechanism should ride on top of this already substantial compound cross section.

So let me describe the results of our trek from 8.5 to 30–40 MeV/u. The reactions we chose are Nb + Be, C, Al in reverse kinematics. As we shall see, the choice of a relatively light target simplifies the picture crucially because of the limitations in impact parameters and in the number of sources. While we explored first the upper part of the energy range at the Bevalac,[7] I shall begin with the lower energy data which we collected at GSI.[8]

Let me use Fig. 8 in part to extoll the advantages of reverse kinematics. In these pictures we see the complex particles events displayed in the Z-E plane. The remarkable double ridge is due to a simple kinematic effect. A single source is emitting fragments in the center of mass with energies independent of direction. Because of the large center-of-mass velocity, a given lab angle intersects the kinematic circle <u>twice</u> giving rise to a double solution. This simple observation allows any person of good sense to conclude that the process is binary, especially when for the measured velocities one obtains a Coulomb-like Z dependence for the center-of-mass velocities. For the remaining St. Thomases we took coincidence data with another detector placed symmetrically on the other side of the beam. These data are shown in Fig. 9 and demonstrate properly that the process is indeed binary, and that an upper solution fragment in one detector is in coincidence with a lower solution fragment in the other.

The pattern seen in Fig. 8 evolves regularly and smoothly with bombarding energy and target. This indicates that indeed we are observing the same kinematic circle, boosted by different velocities of the center-of-mass which are in approximate agreement with those expected from complete fusion. Furthermore, reverse kinematics allows us to verify that what you see is all there is. When we go to wider angles we lose the intersection with the kinematic circle and we see nothing. So there are no other processes than the one we have described, and we can conclude that, up to 18.5 MeV/u "nihil sub sole novi," nothing new under the sun but the old compound nucleus decay.

Proceeding to the better analyzed Bevalac data, we see more of the same. In Fig. 10 the invariant cross sections plotted in the Z-V plane show that the double solutions are retained up to 30 MeV/u. Notice also that at very low Z's there is a trail of low velocity events which we call "big foot." This process is clearly target related, and may have to do with the onset of incomplete fusion. In this case the events are due to the target picking up a few nucleons for the projectile and a corresponding fraction of the momentum.

The velocities of the source are shown in Fig. 11 and clearly indicate a single source for all Z's with a velocity intermediate between the projectile velocity and the compound nucleus velocity but closer to the latter. The inferred incomplete momentum transfer in the direct kinematic solution is in good agreement with the standard momentum transfer systematics. Similarly the velocities in the center of mass are Coulomb-like as shown in Fig. 12.

An example of charge distribution is shown in Fig. 13 together with an absolute calculation. The ability to fit the absolute cross sections vs. Z with a compound nucleus model is in our eyes very significant, because it implies a statistical branching ratio between complex fragment emission and the dominant n, p, ^{4}He decay.

The coincidence data are shown in Fig. 14. The hatched bands are predicted on the basis of the incomplete momentum transfer, of the resulting excitation energy, and of the sequential evaporation from the binary fragments calculated from the code PACE.[9] The overall picture is

consistent with binary decay. However notice that in the case of the Al target at 30 MeV/u a number of events falls outside the expected band, indicating perhaps three or more body decay. A better appreciation of the coincidence data and of the calculations is given in Fig. 15 where the average sum of charges is plotted versus one of the charges. The dashed line is the primary sum inferred from the source velocity and the solid line is the calculation from PACE of the sequential charge evaporation. The excellent agreement indicates a solid understanding of the incomplete fusion process, of the energy deposition, and of the binary decay followed by sequential evaporation. A summary of the GSI and Bevalac data is given in Fig. 16 where the sum of the charges at symmetry is plotted vs. the energy per nucleon. The solid line gives the sum of the target and projectile charges, the long dashed line the compound nucleus charge as obtained in incomplete fusion, and the short dashed line the final sum of charges after sequential evaporation. Up to here, again, the compound nucleus process appears to be the dominant if not the only mechanism of complex fragment production.

Conclusion:

What we can state with a good degree of confidence is that up to the highest explored energy, compound nucleus decay is by far the main source of complex fragments. An additional source at low A's is the "big foot" which is target related and seems to be consistent with the target picking up a few nucleons for the projectile and decaying in its turn. The very thorough exploration of angle and energy "phase space" allowed by reverse kinematics does not leave much room for any other processes. Can we conclude then that they are not there? I think we must wait for ternary and quaternary events which will undoubtedly appear at higher energies. However even with these events one needs to be cautious. Ternary, quaternary and higher multiplicity events can originate from sequential binary decays. In fact, once one has a good excitation function for the binaries, it is a simple exercise to predict the rate of sequential ternaries and quaternaries. This will be the background, and it will not be small, on top of which we shall have to look in search of fancier mechanisms.

APPENDIX

MOMENTUM TRANSFER IN INTERMEDIATE ENERGY COLLISIONS

The extensive measurements of momentum transfer in intermediate energy heavy ion collisions demand an elucidation of the essential kinematic and dynamic features of the associated interaction.

Let us consider the following greatly simplified model. Two nuclei of mass A and B collide in such a way that the nucleus B occludes a portion α of A and, correspondingly, A occludes a portion β of B. Let $\Delta\alpha$ and $\Delta\beta$ be the separation energies of the occluded parts α and β from their respective nuclei A and B.

The following questions arise:

I. If $\Delta\beta = \infty$

1) What is the minimum energy with which B must strike A so that the occluded portion α is shaved off and attaches itself to B?

2) At any higher energy than calculated in 1) what is the momentum of A$-\alpha$ and B$+\alpha$? Similarly, if $\Delta\alpha = \infty$ one can ask the questions symmetric to the ones above.

II. If neither $\Delta\alpha$ nor $\Delta\beta = \infty$

1) At what energy will any of the pieces α,β be shaved off?

2) At what energy will both of the pieces α,β be shaved off?

It is simple to show that the questions based in I have an answer that is purely kinematical and independent on the dynamics while the questions posed in II do require a solution of the dynamical problem. In other words the answers to I require solely the knowledge of A, B, α, β, $\Delta\alpha$, $\Delta\beta$, while the answers to II require additional information like restoring forces etc. Unfortunately this additional information is strongly model-dependent. However some illumination is already provided by answering the easier questions in I.

Let us consider first the case of A at rest being hit by B with momentum P. If the piece α sticks to B we have for the momentum of A -

α and $B + \alpha$

$$\frac{P_{A-\alpha}}{P} = \frac{m^*_\alpha}{B + \alpha}\left(1 - \sqrt{1 - \frac{2\Delta\alpha}{m^*_\alpha v_0^2}}\right)$$

$$\frac{P_{B+\alpha}}{P} = 1 - \frac{m^*_\alpha}{B + \alpha}\left(1 - \sqrt{1 - \frac{2\Delta\alpha}{m^*_\alpha v_0^2}}\right)$$

where

$$m^*_\alpha = \frac{(B + \alpha)(A - \alpha)}{A + B} \quad ;$$

$$v_0 = \frac{B}{B + \alpha} v \quad ;$$

$$v = \frac{P}{B}$$

The complementary case involves again A being at rest, but, this time, picking up a piece β from the projectile B. We have

$$\frac{P_{A + \beta}}{P} = \frac{\beta}{B}\left[1 + \frac{A(B - \beta)}{(A + B)\beta}\left(1 - \sqrt{1 - \frac{2\Delta\beta}{m^*_\beta v_0^2}}\right)\right]$$

$$\frac{P_{A + \beta}}{P} = \frac{B - \beta}{B}\left[1 - \frac{A}{A + B}\left(1 - \sqrt{1 - \frac{2\Delta\beta}{m^*_\beta v_0^2}}\right)\right]$$

where

$$m^*_\beta = \frac{(A + B)(B - \beta)}{A + B} \quad ;$$

$$v_0 = \frac{A}{A + \beta} v \quad ;$$

$$v = \frac{P}{B} \quad .$$

It is interesting to notice that full momentum transfer (no shaving off of α or β) occurs when the square roots vanish, or when

$$\frac{2\Delta\alpha}{m_\alpha^* v_0^2} = 1 \quad ; \quad \frac{2\Delta\beta}{m_\alpha^* v_0^2} = 1 \quad .$$

This occurs when the energy of B is

$$\frac{E}{B} = \Delta\alpha \frac{(B + \alpha)(A + B)}{(A - \alpha)B^2} \quad ;$$

$$\frac{E}{B} = \Delta\beta \frac{(A + \beta)(A + B)}{(B - \beta)A^2}$$

Notice also that at asymptotically large energies the momentum transfers tend to those one would have without binding, or $\Delta = 0$.

In the spirit of the geometrical model one can attempt to calculate α, β, $\Delta\alpha$, $\Delta\beta$ from the impact parameter. The quantities α,β are given by as reported in Ref. 10. For the quantities $\Delta\alpha$, $\Delta\beta$ we can take the energy of the new surface created by the abrasion process. For this we need to calculate the area of lateral surface defined by a cylinder and a sphere of radii r and R at an impact parameter b. If S is such a lateral area the total new surface created is 2S. The area S can be obtained analytically

$$S = 8r \sqrt{R^2 - r^2 - b^2 + 2br}\ E\left(\frac{\pi}{2},k\right)$$

$$k = \sqrt{\frac{2br}{R^2 - r^2 - b^2 + 2br}}$$

for $R^2 - r^2 - b^2 > 2\ br \geq 0$, and

$$S = 4r \sqrt{\frac{1}{br}} \left\{(R^2 - r^2 - b^2 - 2br) \times F\left(\frac{\pi}{2},\frac{1}{k}\right) + 4br\ E\left(\frac{\pi}{2},\frac{1}{k}\right)\right\}$$

for $|R^2 - r^2 - b^2| < 2\ br$, where E,F are the elliptic integrals of 1st and 2nd kind. As an example let us consider the reaction Be + Nb.

Figure 17 demonstrates the impact parameters at which incomplete fusion processes become energetically possible for Be and Nb breakup. The area below each curve corresponds to the fragmentation region; above each curve is the complete fusion region. At impact parameters less

than 3.5 fm the Be projectile is completely occluded by the Nb target; hence, Be fragmentation does not occur. Note that at all impact parameters less energy is required to shatter Be due to the smaller surface area created.

Figure 18 shows the fraction of the initial momentum in the target-like (Nb) fragment as a function of bombarding energy per nucleon. The momentum transfer was calculated assuming projectile (Be) breakup at various impact parameters. Figure 19 is the complement of Fig. 2 showing the fractional momentum in the projectile residue. As would be expected, central collisions lead to larger momentum transfer. In the limit of large bombarding energies the momentum transfer at any given impact parameter tends to a constant as $\frac{\Delta\alpha}{E_{lab}} \rightarrow 0$.

Acknowledgement:

This work was supported by the Director, Office of Energy Research, Division of Nuclear Physics of the Office of High Energy and Nuclear Physics of the U.S. Department of Energy under Contract DE-AC03-76SF00098.

References:

1. J. Aichelin and J. Huefuer, Phys. Lett. 136B, 15 (1984).
2. See for instance, J. E. Finn et al., Phys. Rev. Lett. 49, 1321 (1982).
3. L.G. Moretto, Nucl. Phys. A247, 211 (1975).
4. M.A. McMahan et al., Phys. Rev. Lett. 54, 1995 (1985).
5. A.J. Sierk, Phys. Rev. Lett. 55, 582 (1985).
6. L.G. Sobotka et al., Phys. Rev. Lett. 53, 2004 (1984).
7. R.J. Charity et al., LBL-20383, and Phys. Rev. Lett., March 30, 1986
8. R.J. Charity et al., to be published.
9. A. Gavron, Phys. Rev. C21, 230 (1980).
10. W.J. Swiatecki, as published in appendix by J. Gosset et al., Phys. Rev. C16, 629 (1977).

Figure Captions:

Figure 1. Schematic representation of the ridge line or of the locus of conditional saddle points at fixed mass asymmetry.

Figure 2. Comparison of the potential energy surfaces (solid curve) and expected yields (dashed curve) for a) a heavy CN (Au at $\ell = 0$ and $E^* = 97$ MeV) and b) a light CN (Ge at $\ell = 0$ and $E^* = 72$ MeV).

Figure 3. Invariant cross section plots $\left[\propto \frac{1}{V^2} \frac{d^2\sigma}{d\Omega dV}\right]$ for representative ejectiles (Li, ^{9}Be, B, and C). The diameter of the dots is proportional to the logarithm of the cross section and the X's indicate the peak of velocity distribution. The two large arcs are sections of circles centered on the c.m. velocity (center arrow) appropriate for complete fusion. The beam direction (0°) is indicated by the c.m. velocity vector.

Figure 4. Dependence of the total integrated cross sections for emission of complex fragments on the center-of-mass energy, $E_{c.m.}$ in the reaction ^{3}He + nat$_{Ag}$. The points and error bars correspond to the experimental cross sections. The curves are fits with the parameters of Fig. 5.

Figure 5. The emission barriers, B_z, extracted in fitting the excitation emission of complex fragments functions as a function of fragment charge. The liquid drop model and finite range model calculations are from Ref. 5.

Figure 6. The deduced c.m. energies (filled circles) and source velocities (open symbols) for the ^{93}Nb + ^{12}C system. Source velocities were determined assuming that the product mass followed the line of β-stability (open circles) or the charge equilibration line (open squares). A Coulomb calculation for two spheres is shown both for the c.m. energy of the light fragment (solid line) and the total kinetic energy (dashed line). The value of the source velocity expected for full momentum transfer is indicated by the horizontal line.

Figure 7. Center-of-mass cross sections for products from the ^{74}Ge, ^{93}Nb and ^{193}La + ^{9}Be systems detected at $\theta_{Lab} = 7.5$. The solid line is a liquid drop model calculation of the fragment yield at $\theta_{c.m.} = 30$. The arrows indicate the entrance channel asymmetry. See text. Data below $z_{asy} = 0.15$ were not obtained for the La + Be system, due to a limited dynamic range of the telescope.

Figure 8. Scatter plot of charge vs. energy for singles events produced in the reaction 18.5 MeV/u ^{93}Nb + ^{9}Be. The detector subtended angles from 4° to 12°. The two dark bands correspond to Coulomb emission from a compound nucleus forward and backward in the center-of-mass.

Figure 9. Coincidences between two telescopes at identical angles on the opposite side of the beam. Because of the symmetric location of the detectors, the coincidence measurements select out events corresponding

to symmetric division of the compound nucleus.

Figure 10. Singles distribution of reaction products plotted as logrithmic contours of invariant cross section $[(1/V^2)(\partial^2\sigma/\partial\Omega\partial V)]$ in the Z-velocity plane. The arrows indicate the velocities for 1) full momentum transfer 2) the experimentally determined momentum transfer and 3) the beam. Calculated (dashed lines) average velocities of complex fragments for the maximum and minimum lab angles of the telescope (3° and 8°) are indicated.

Figure 11. Measured source velocities vs. fragment charge for the system 25 MeV/u ^{93}Nb + ^{27}Al. The solid line is the source velocity averaged over Z. The dashed line is the velocity corresponding to complete fusion of projectile and target.

Figure 12. Velocities of fragments in the center-of-mass for 25 and 30 MeV/u ^{93}Nb + ^{9}Be. The solid lines show Coulomb calculations for two spheres with a separation of $R = 1.224(A_1^{1/3} + A_2^{1/3}) + 2$ fm).

Figure 13. Angle-integrated cross sections (symbols) for complex fragments emitted from the reaction 30 MeV/u ^{93}Nb + ^{27}Al and ^{9}Be. Liquid-drop model calculation (solid line) of the fragment yield for the latter system.

Figure 14. Scatter plots of coincidence events between the 5.5° telescope (Z_1) and the −11° telescope (Z_2). The shaded areas represent an estimation of regions where binary events should lie following sequential evaporation from the primary fragments.

Figure 15. The mean sum, $\langle Z_1 + Z_2 \rangle$ of coincidence events (solid symbols) plotted as a function of Z_2. The dashed lines indicate the average charge of the compound system as estimated from the mass transfer. The charge loss of binary events, due to sequential evaporation, was estimated using the PACE[9] code and the residual $\langle Z_1 + Z_2 \rangle$ values are indicated by the solid curves.

Figure 16. The solid circles show the average sum of the charges ($\langle Z_1 + Z_2 \rangle$) for nearly symmetric complex fragments measured in coincidence from the reaction ^{93}Nb + ^{27}Al as a function of bombarding energy. The curve labelled Z_{CN} represents the average charge of a compound system formed in an incomplete fusion reaction. It was calculated using the known systematics of momentum transfer. The charge lost due to evaporation from the primary fragments was calculated with PACE. The calculated residual charge ($Z_{CN} - Z_{evaporated}$) of the two fragments (short dashed curve) is in excellent agreement with the data.

Figure 17. Incomplete fusion processes occur below each curve (see text).

Figure 18. Momentum of Nb-like fragment after Be breakup.

Figure 19. Momentum of Be-like fragment after Be breakup.

Evaporation of Complex Fragments or Fission along the Mass Asymmetry Coordinate

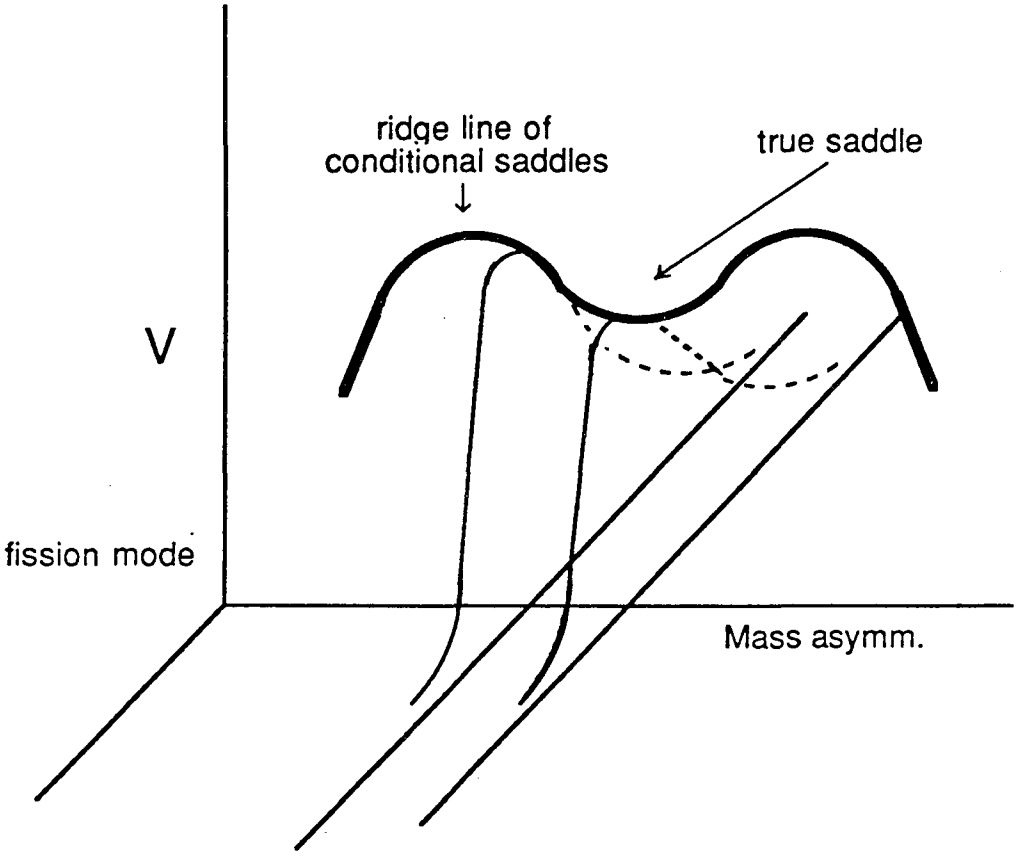

Fig. 1

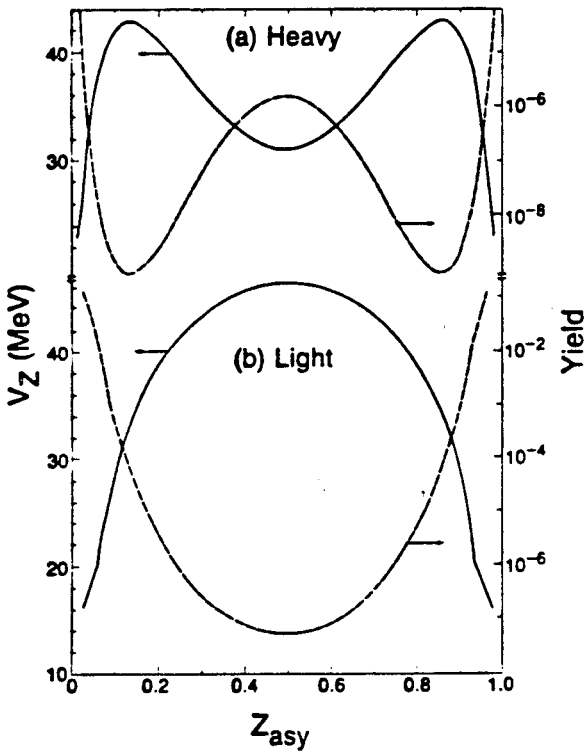
(a) Heavy
(b) Light
V_Z (MeV)
Yield
Z_{asy}
40
30
20
10
0
0.2
0.4
0.6
0.8
1.0
10^{-6}
10^{-8}
10^{-2}
10^{-4}
10^{-6}

Fig. 2

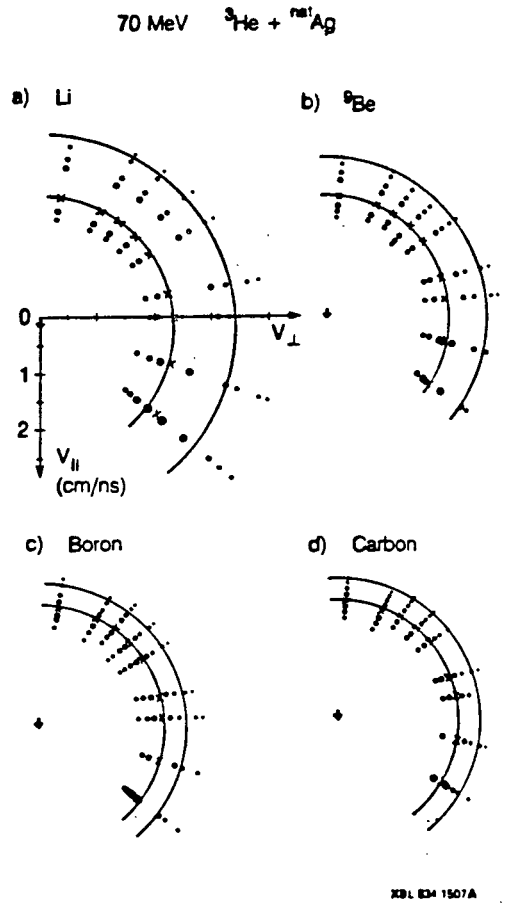
70 MeV ^{3}He + ^{nat}Ag
a) Li
b) ^{9}Be
c) Boron
d) Carbon
$V_\perp$
$V_{\parallel}$
(cm/ns)
0
1
2
XBL 834 1507A

Fig. 3

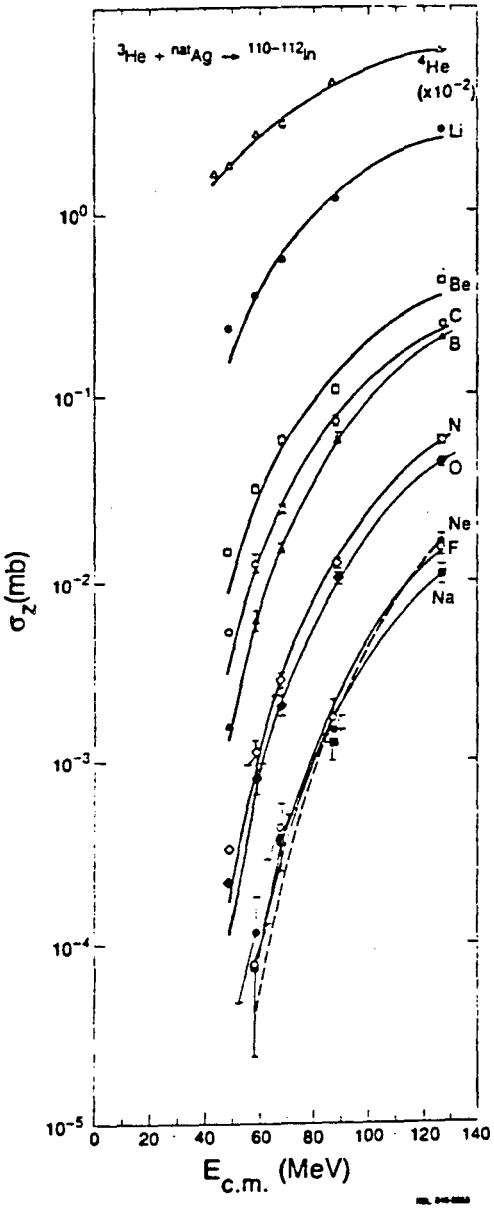
^{3}He + ^{nat}Ag → $^{110-112}$In
^{4}He (x10^{-2})
Li
Be
C
B
N
O
Ne
F
Na
σ_Z(mb)
$E_{c.m.}$ (MeV)

Fig. 4

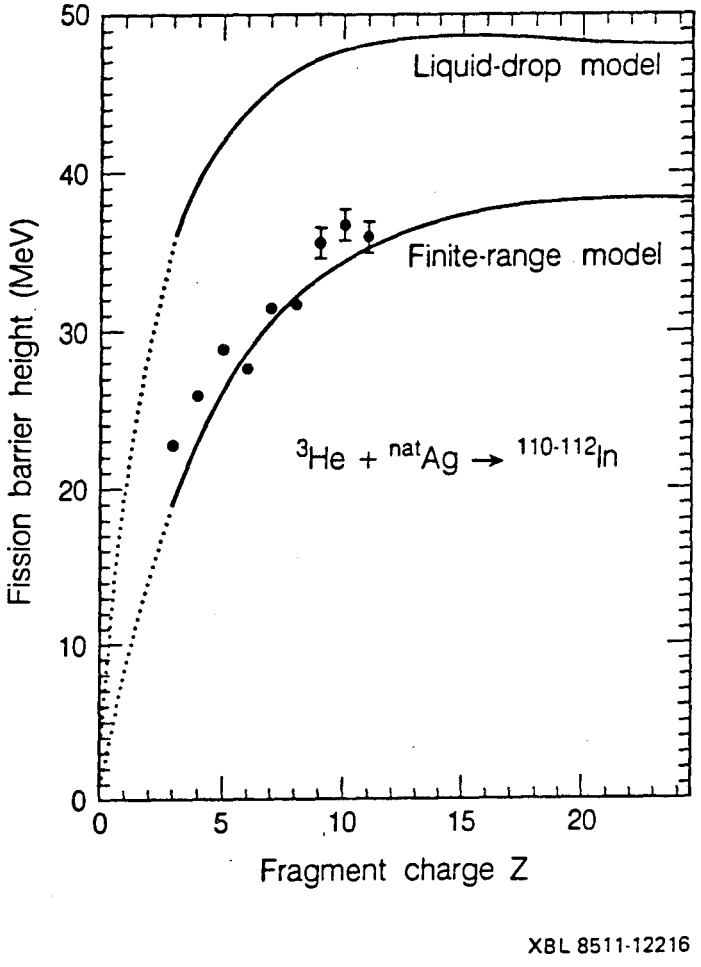
Liquid-drop model
Finite-range model
^{3}He + ^{nat}Ag → $^{110-112}$In
Fission barrier height (MeV)
Fragment charge Z
XBL 8511-12216

Fig. 5

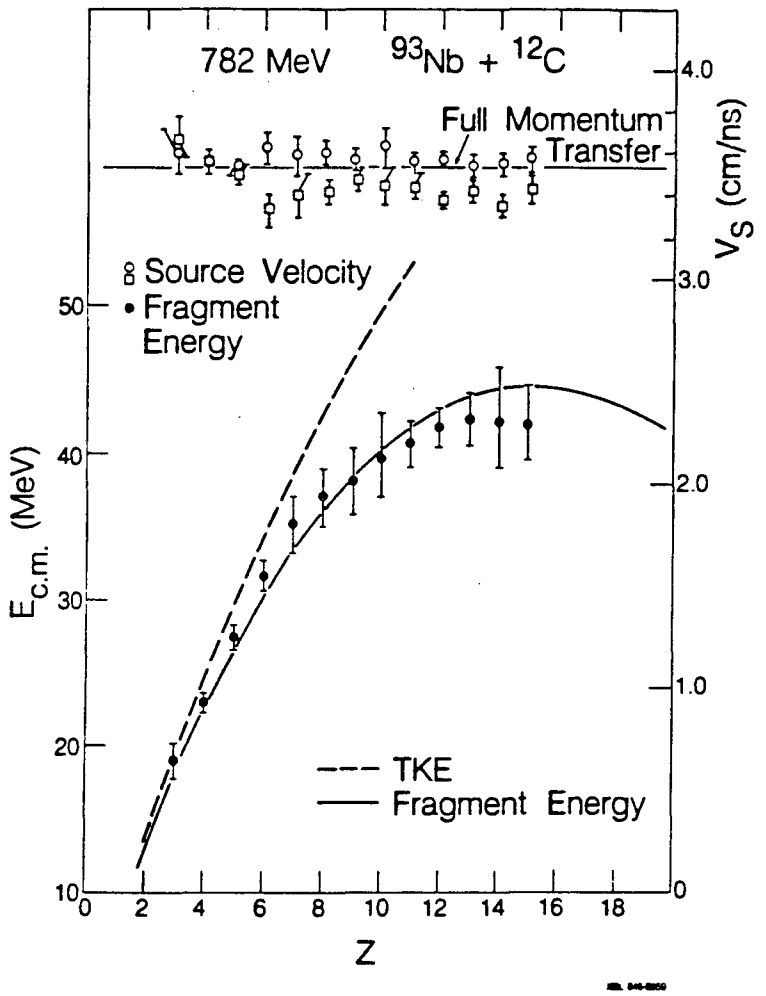
782 MeV
93Nb + 12C
Full Momentum Transfer
Source Velocity
Fragment Energy
TKE
Fragment Energy
E c.m. (MeV)
V S (cm/ns)
Z

Fig. 6

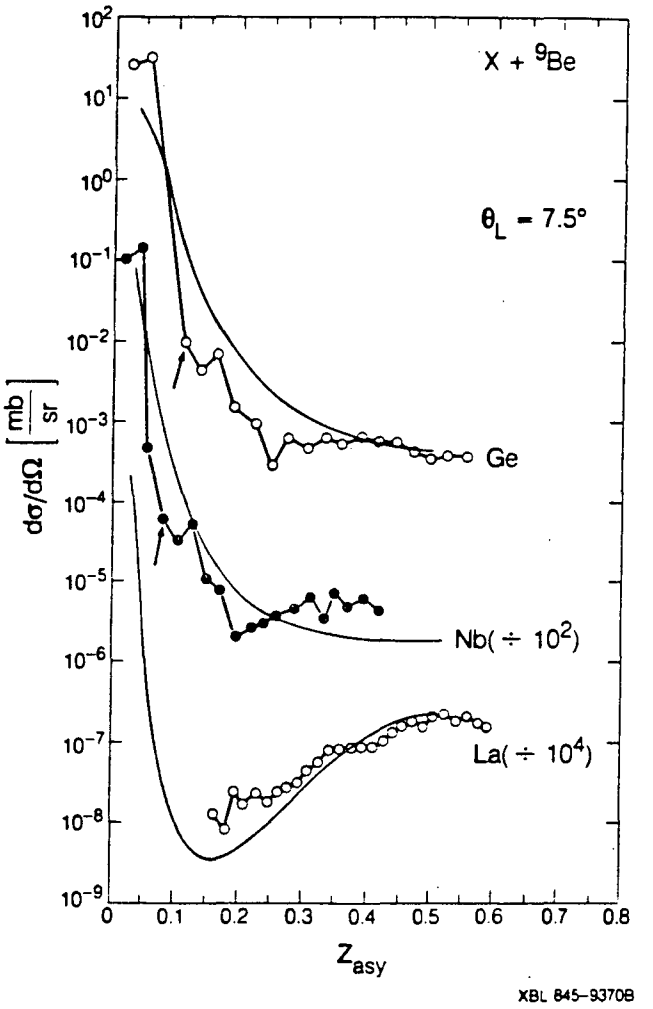
X + 9Be
θL = 7.5°
Ge
Nb(÷ 10^2)
La(÷ 10^4)
dσ/dΩ [mb/sr]
Z asy
XBL 845-9370B

Fig. 7

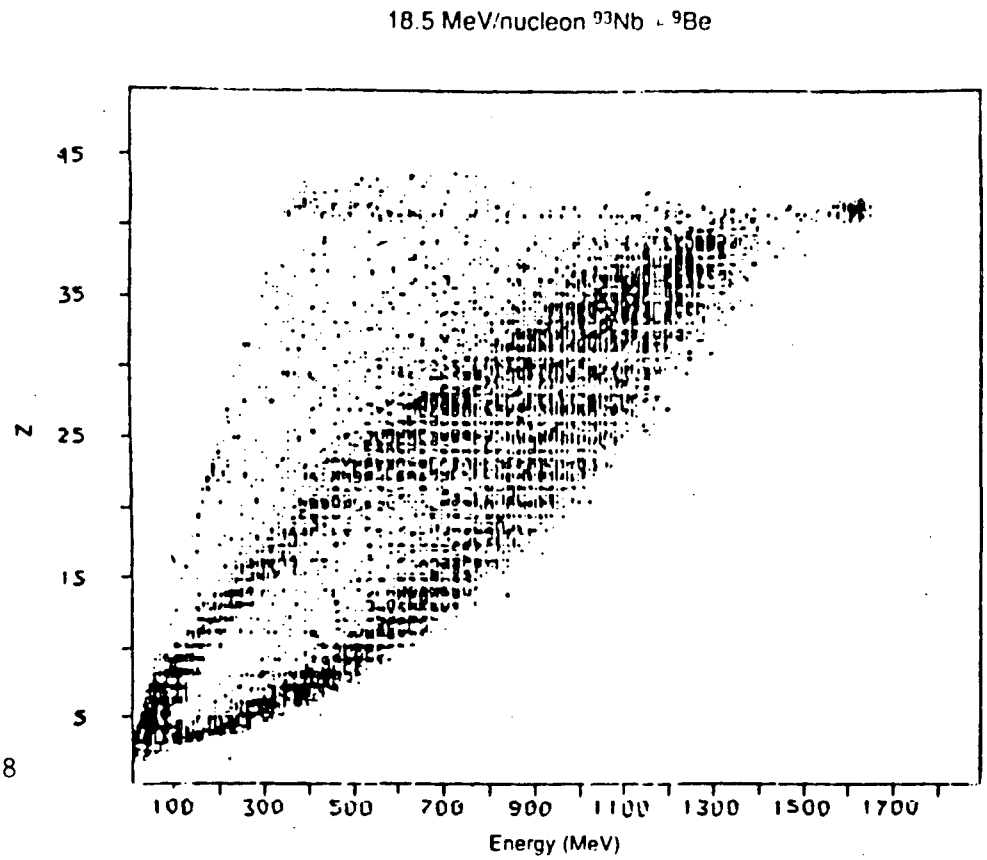
18.5 MeV/nucleon ^{93}Nb + ^{9}Be
45
35
25
15
5
Z
100
300
500
700
900
1100
1300
1500
1700
Energy (MeV)

Fig. 8

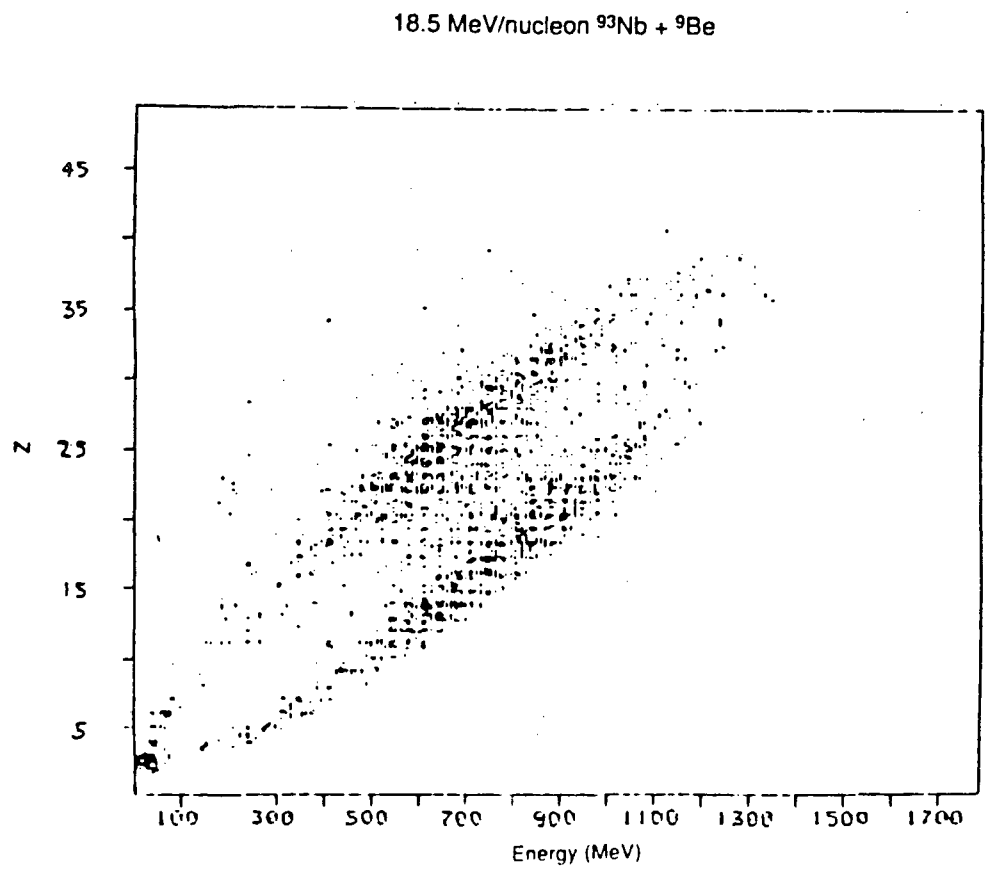
18.5 MeV/nucleon ^{93}Nb + ^{9}Be
45
35
25
15
5
Z
100
300
500
700
900
1100
1300
1500
1700
Energy (MeV)

Fig. 9

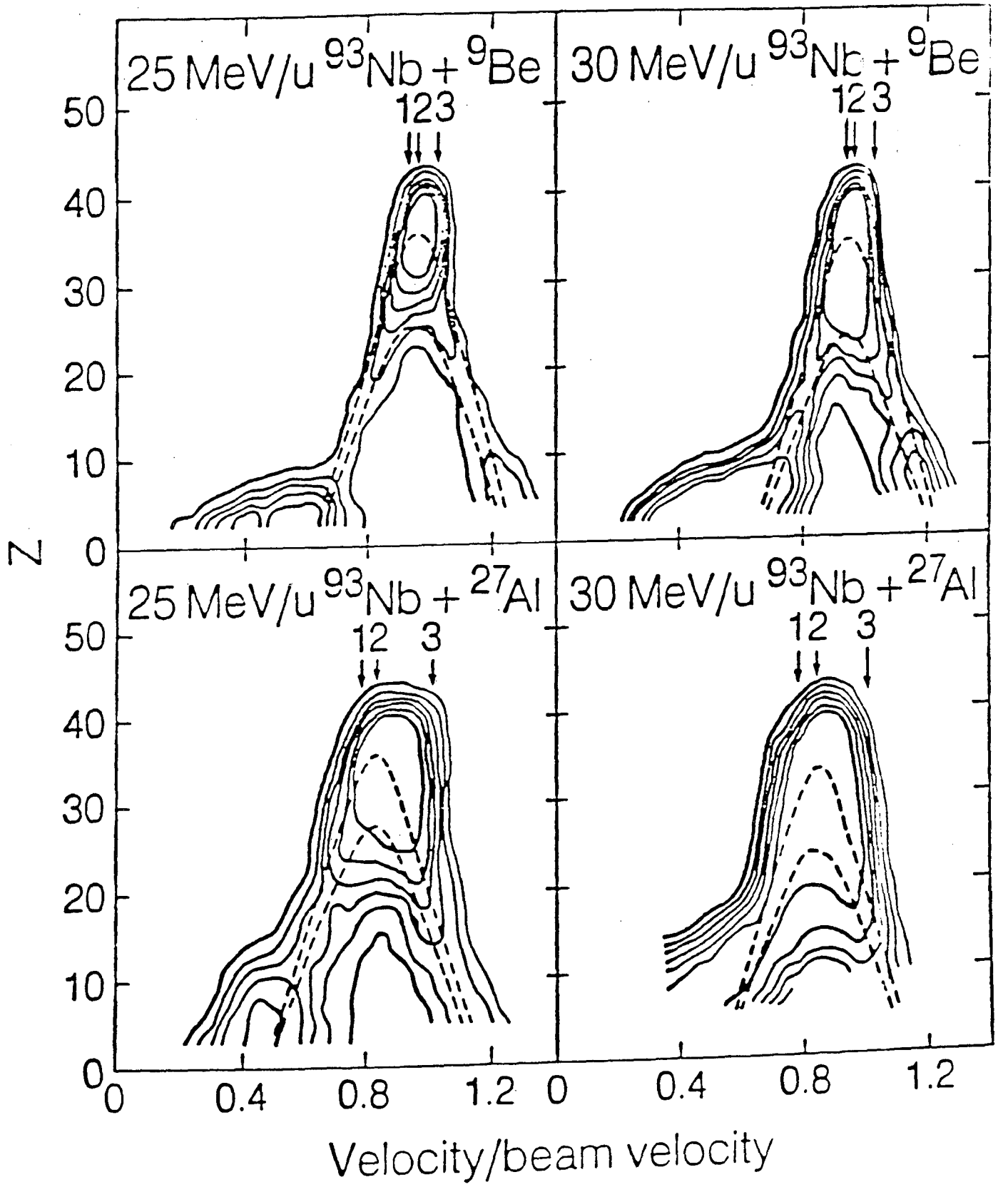
25 MeV/u ^{93}Nb + ^{9}Be
123
30 MeV/u ^{93}Nb + ^{9}Be
123
25 MeV/u ^{93}Nb + ^{27}Al
12 3
30 MeV/u ^{93}Nb + ^{27}Al
12 3
N
0
10
20
30
40
50
0
0.4
0.8
1.2
Velocity/beam velocity

Fig. 10

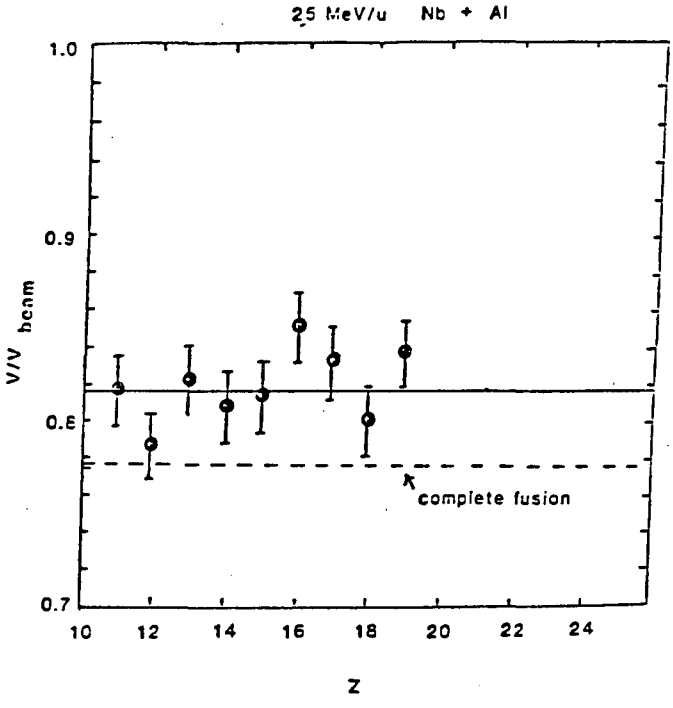
25 MeV/u Nb + Al
1.0
0.9
0.8
0.7
V/V beam
complete fusion
10
12
14
16
18
20
22
24
Z

Fig. 11

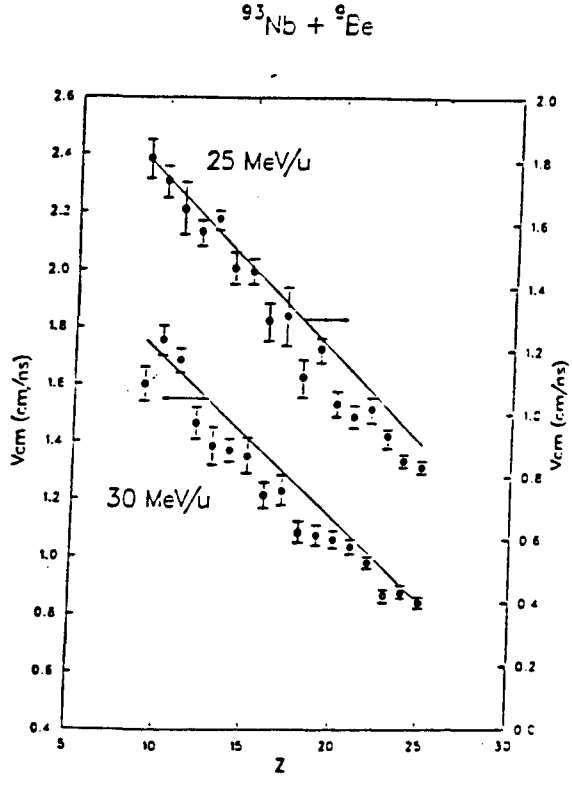
93Nb + 9Be
25 MeV/u
30 MeV/u
Vcm (cm/ns)
Vcm (cm/ns)
Z

Fig. 12

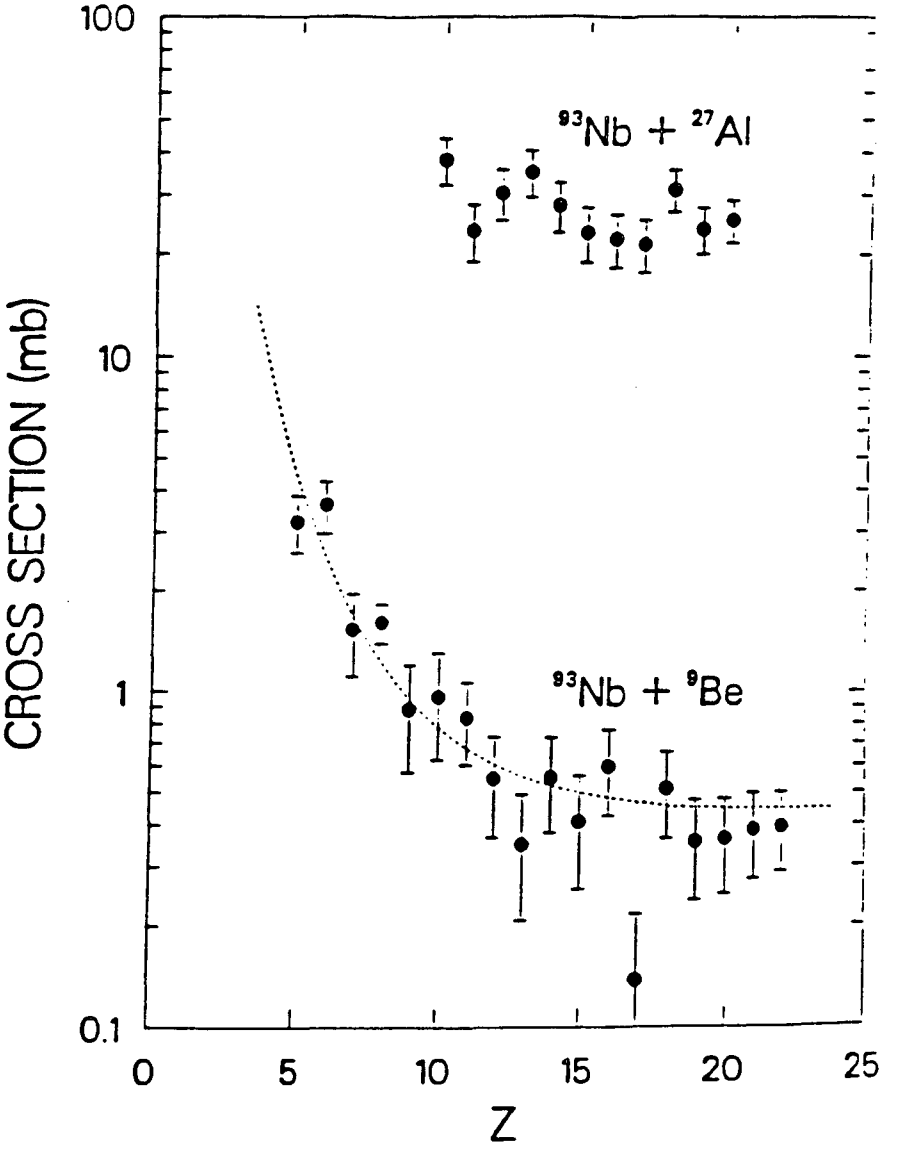

Fig. 13

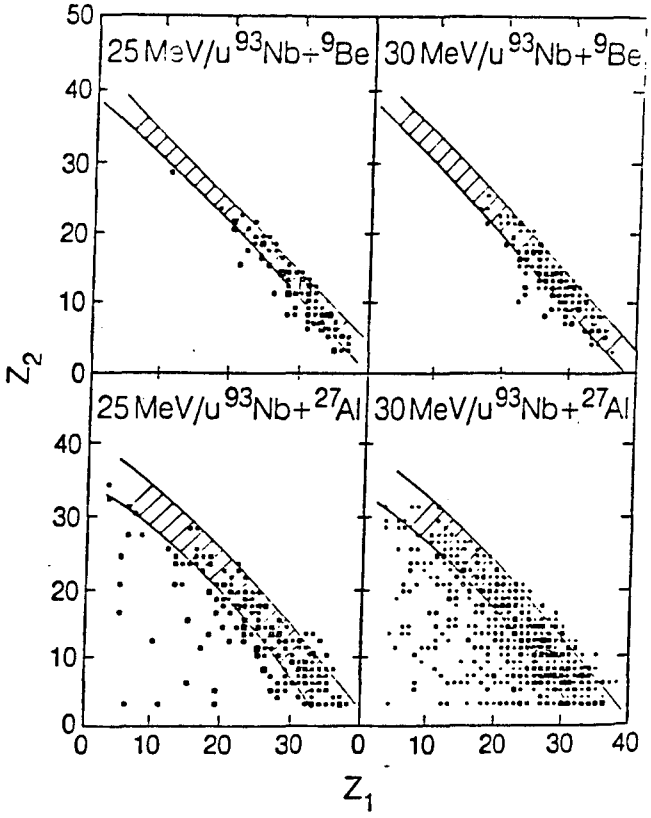

XBL 859-8976

Fig. 14

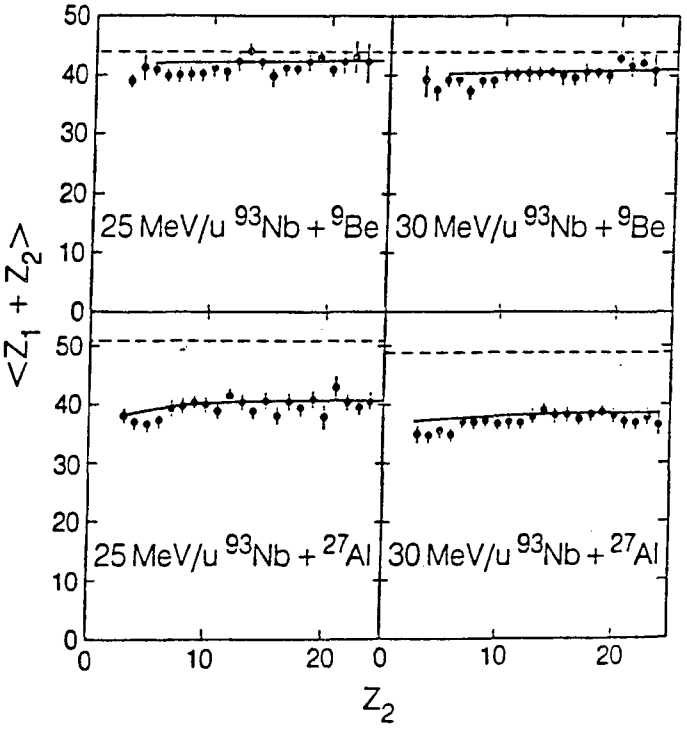

XBL 859-8977

Fig. 15

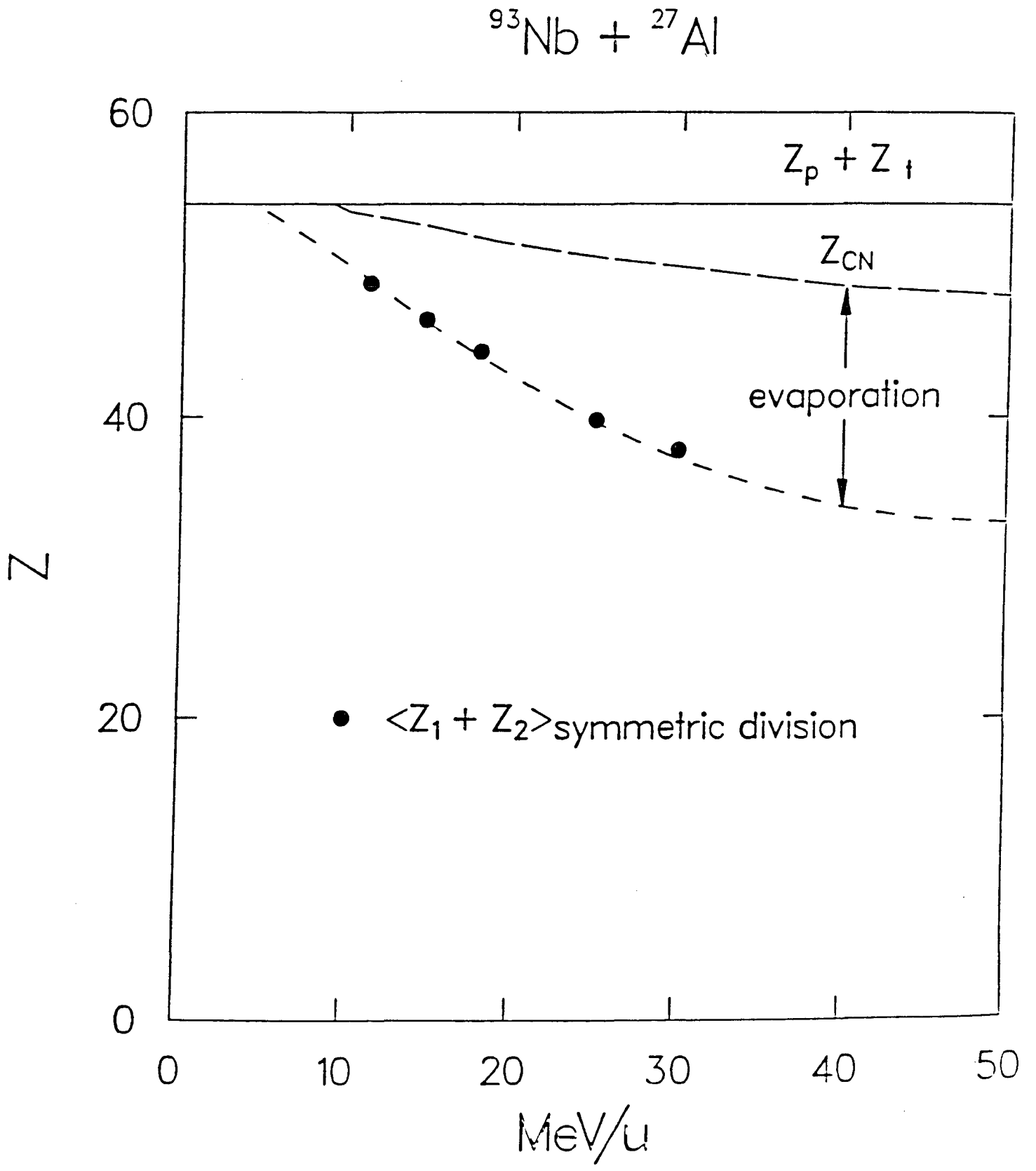
$^{93}Nb + ^{27}Al$
60
40
20
0
Z
$Z_p + Z_t$
Z_{CN}
evaporation
$\langle Z_1 + Z_2 \rangle$symmetric division
0
10
20
30
40
50
MeV/u

Fig. 16

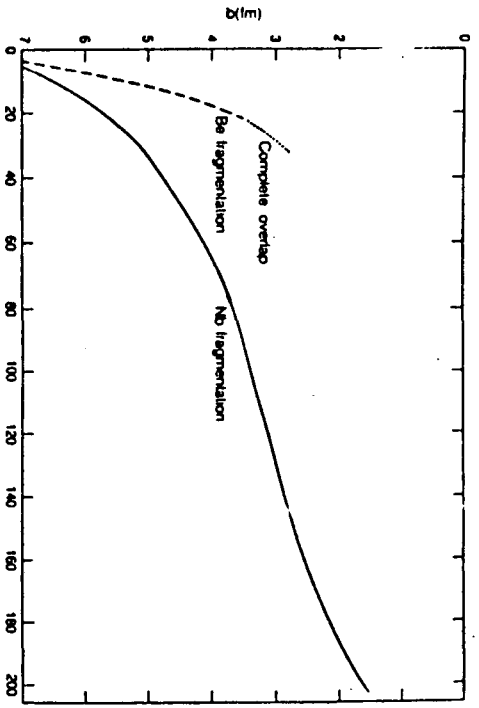

Fig. 17

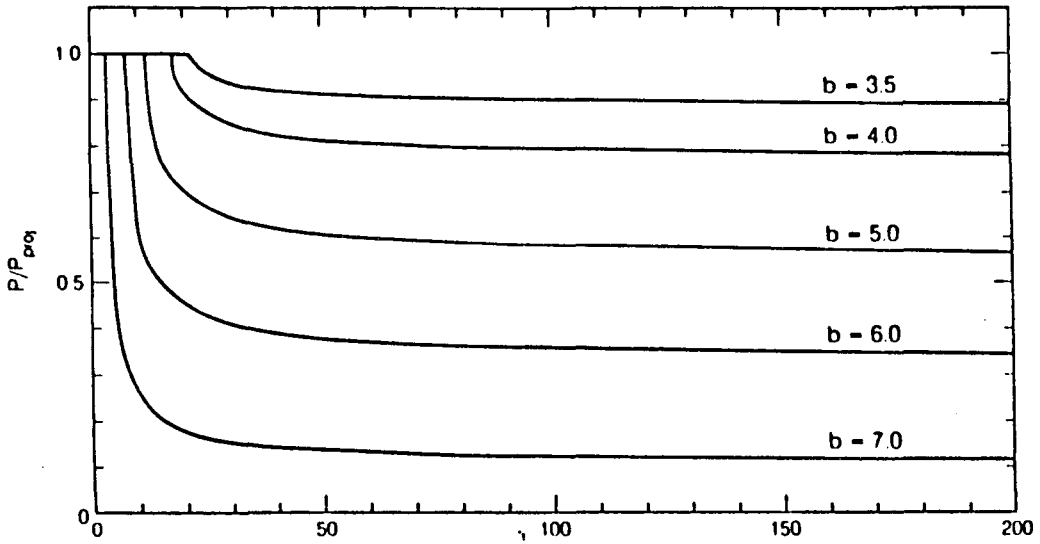

Fig. 18

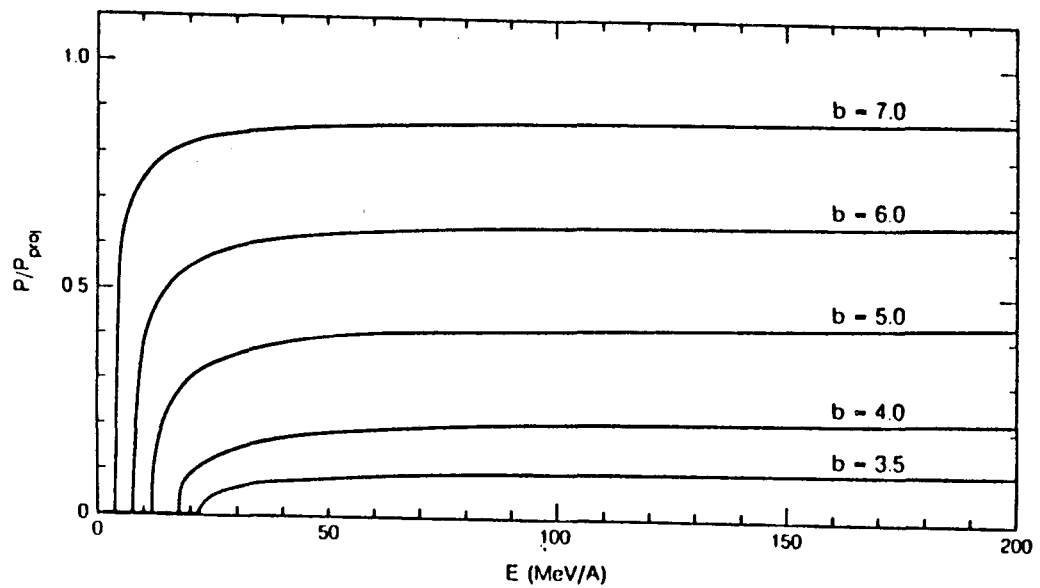

Fig. 19

This report was done with support from the Department of Energy. Any conclusions or opinions expressed in this report represent solely those of the author(s) and not necessarily those of The Regents of the University of California, the Lawrence Berkeley Laboratory or the Department of Energy.

Reference to a company or product name does not imply approval or recommendation of the product by the University of California or the U.S. Department of Energy to the exclusion of others that may be suitable.

LAWRENCE BERKELEY LABORATORY
TECHNICAL INFORMATION DEPARTMENT
UNIVERSITY OF CALIFORNIA
BERKELEY, CALIFORNIA 94720